Crystallization Kinetics and Crystal Structure of Nylon6-Clay Nanocomposites: Combined Effects of Thermomechanical History, Clay Content, and Cooling Conditions

V. Miri,[†] S. Elkoun,[†] F. Peurton,[†] C. Vanmansart,[†] J.-M. Lefebvre,[†] P. Krawczak,[‡] and R. Seguela*[,†]

Laboratoire de Structure et Propriétés de l'Etat Solide, UMR CNRS 8008, Université de Lille 1, Batiment C6, 59655 Villeneuve d'Ascq, France, and Dept. Technologie des Polymeres et Composistes et Ingenierie Mecanique, Ecole des Mines, 59508 Douai, France

Received August 7, 2008; Revised Manuscript Received October 1, 2008

ABSTRACT: The crystallization behavior and the crystalline structure of nylon6-clay nanocomposites are investigated with regard to the processing conditions and thermal treatment. Microextruded bulk samples as well as blown films are under concern. The often reported nucleating effect of the clay particles is shown to strongly depend on the processing parameters prior to the solidification step, namely, the shear intensity which promotes self-nucleation and the temperature of the melt which regulates the density of these unstable nuclei. The MMT content influences the crystallization kinetics and the crystalline structure via the shear amplification phenomenon which increases the densities of both the shear-induced and the MMT-induced nuclei. The MMT platelets also turned out to hinder the crystal growth. The cooling rate plays a major role on the final crystalline structure by shifting the crystallization temperature in the specific growth range of either the α- or the γ-crystal forms of the nylon6 matrix. Blown films corroborate the findings from microextruded samples regarding the competition between nucleation and growth in the resulting crystalline form of the nylon6 matrix. Besides, the strong texturing of the nanocomposite films provides information on the local arrangement of the chains and crystal unit cell on the MMT platelets.

Introduction

Polymer-based composites filled with nanometric stiff particles of high form factor have received increasing attention since the early 90s due to spectacular increase in mechanical properties with regard to the neat matrix, together with strongly improved fire retardancy and great potential for barrier properties.[1−3] Clays and related natural or synthetic phyllo-silicates are the most commonly used nanofillers, generally surface-treated with organic compounds for improving dispersion in the polymer matrix. Regarding the mechanical behavior of the so-called nanocomposites (NCs), stiffness and heat distortion temperature (HDT) are remarkably enhanced in comparison with the neat polymer matrices, and conventional composites as well at equivalent filler content. The property improvement is yet highly dependent on the physicochemical nature of the matrix. If the stiffness of elastomers is strongly enhanced by clay compounding,[4,5] glassy polymers display moderate stiffening that depends on the degree of dispersion and the particle aspect ratio.[6−8] Brittle thermosetting polymers may exhibit enhanced stiffness and toughness,[9,10] but the actual mechanism of toughening not identified.

NCs based on semicrystalline thermoplastic matrices behave differently depending on the filler−matrix interactions. Polyolefins[11−13] need compatibilization with a polar-functionalized polymer to improve matrix−filler interactions that govern both organoclay clay dispersion and polymer−clay adhesion. However, up to now, the issues turned out little satisfactory regarding use properties. Polyesters[14−16] have more favorable interactions with usual organoclays that provide mechanical property enhancement at low clay content, depending on the clay dispersion. Intrinsically, hydrophilic polymers such as nylons display high matrix−particle interactions both in the melt and in the solid state. This results in high degree of clay dispersion, up to complete exfoliation, and much efficient improvement of thermomechanical properties as revealed by the dramatic increase in HDT.[1−3,17−19] However, the longer the aliphatic segments of the nylon chains the poorer the clay dispersion due to reduced concentration of polar groups.[20]

Nylon6-based NCs have been the scope of much more investigations than any other system. In this domain, montmorillonite (MMT) surface-treated with various types of alkylammonium surfactants has been the most currently used type of clay. The γ-nucleating effect of MMT has been widely reported and often ascribed to epitaxial crystal growth.[21−31] However, the fact that various kinds of nanometric fillers with different chemical nature and crystallographic characteristics, such as mica,[32] sepiolite,[33] zinc oxide,[34] glassy fluorophosphate,[35] or metallic silver,[36] have the same γ-nucleating effect on the nylon6 matrix suggests that surface energy rather than actual epitaxy is more likely involved in the phenomenon. Moreover, several authors have reported that α-form crystals may be predominant over γ-crystals in the presence of MMT, depending on thermal history and thermomechanical treatment.[23,37−44] Notwithstanding, evidence were provided that, even when both γ- and α-crystals are present, the former ones are closer to the particle surface than the latter ones, corroborating the actual influence of clay on the preferred nucleation of γ-crystals,[23,45,46] not necessarily the actual epitaxy. This is also supported by the fact that γ-crystals have been shown to appear first during slow cooling from the quiescent melt before the predominant development of α-crystals upon further cooling.[47] It is worth noticing that various kinds of micro- and nanofillers such as amorphous silica,[48,49] polyhedral-oligomeric-silsesquioxane (POSS),[50] talc,[51] graphite,[52] and multiwall carbon nanotubes[53−56] have been reported to promote the α-crystal form of nylon6 under various cooling conditions. Finally, precipitated calcium carbonate displayed ambivalent properties depending

* To whom correspondence should be addressed. E-mail: roland.seguela@univ-lille1.fr.
[†] Université de Lille 1.
[‡] Ecole des Mines.

10.1021/ma801804y CCC: $40.75
Published on Web 10/30/2008

on its own crystalline type:[57] aragonite and calcite are promotive of the α- and the γ-crystal forms, respectively.

In parallel to the nucleating effect, the crystallization kinetics of nylon6 proved to be strongly affected by the presence of clay. However, contradictory findings appeared from the literature data. From both isothermal and nonisothermal crystallization studies, several authors reported an increase of crystallization kinetics that was invariably ascribed to the so-called clay nucleating effect.[22,27,28,37,42,58] In contrast, some observed a clay-induced reduction of the global crystallization rate[59] that might be attributed to the disruption of lamella growth by the well dispersed clay platelets[27] and could eventually challenge the previously mentioned nucleating effect.[37] From a meticulous modulated-DSC analysis, Miltner et al.[60] suggested that polymer−clay interactions reduce chain mobility that benefits to the γ-form growth, depending on the nature of the clay-surfactant.

Regarding the thermomechanical behavior of NCs based on semicrystalline polymer matrix, particularly above the glass transition temperature, the stiffness and HDT improvement has been intuitively ascribed to restricted molecular motions due to the chain confinement.[11,16,17] The characteristic chain dimensions are indeed in the same range as the average interparticle distance when high dispersion or intercalation of clay is achieved. However, conflicting experimental data have also been reported on this topic (see the discussion by Miltner et al., ref 60). Only minor temperature shifts of either the glass transition or the main mechanical relaxation of NCs have been reported with regard to polymer parents.[11,12,18,61,62] This means that short-range chain mobility is not significantly affected in the major part of the polymer matrix as concluded from NMR proton spin diffusion.[63] In contrast, dielectric relaxation measurements[64] and modeling data,[65] regarding intercalated systems, have revealed faster chain dynamics in the amorphous phase confined in the clay galleries. The later findings are corroborated by positron annihilation experiments that revealed increased free volume for large clay amounts.[66] Alternatively, composite theories assuming strong polymer−filler adhesion have been shown to fairly well account for the NCs stiffening due to the high aspect ratio of individual clay particles and clay tactoids as well.[67−71] Besides, several authors suggested that the buildup of a percolating structural network between crystalline component of the polymer matrix and the nanofillers may contribute an additional mechanical coupling.[12,28,72]

To sum up, the competing development of α- and γ-crystals more or less closely connected with the MMT platelets in nylon6-based NCs is likely to have a drastic incidence on the mechanical property improvement. So, more efforts should be paid to the understanding and control of the growth mechanisms of γ and α crystals in these NCs. The present paper aims at investigating the specific role of processing, and cooling conditions on the crystallization kinetics and the development of the various crystalline forms of the nylon6 matrix in a series of nylon6-MMT nanocomposites of various MMT contents.

Experimental Section

The materials from UBE Ltd. (Japan) consisted of neat polyamide6 (PA6) together with two nanocomposites (NCs) containing 2 and 4.5% by weight of montmorillonite (MMT). The two NCs were synthesized by in situ polymerization according to a previously described procedure.[73] The organically modified MMT was prepared by a surface cation exchange reaction with 12-aminolauric acid. The weight-average molar weights are close to 20 kDa after UBE indications. This figure is quite consistent with data reported by Lincoln et al.[23] for the same or very similar materials from UBE Ltd. Four additional NCs having various MMT contents in the range 0−4.5% have been prepared from mixtures of the neat PA6 and either of the two supplied NCs. These materials were compounded in a corotating twin-screw microextruder from DSM (Geelen, The Netherlands). The extrusion parameters were the following: barrel temperature = 250 °C, screw speed = 50 rpm, residence time = 10 min. Prior to the melt-processing, all the systems kept in dry place were heat-treated overnight under vacuum at 80 °C. In some occasions, a screw speed of 5 rpm was used to check the incidence of shear intensity. The extrudates were cooled in air at the exit of the die having a 2 mm diameter. All the samples were subsequently stored in desiccators under vacuum.

Table 1. Expected and Actual Values of the MMT Weight Fraction in the Microextruded Materials

materials	PA6-0	PA6-0.5	PA6-1	PA6-2	PA6-2.5	PA6-3.5	PA6-4.5
expected (w%)	0	0.5	1.0	2.0	2.5	3.5	4.5
actual (w%)	0	0.6	1.1	1.9	2.5	3.4	4.3

Films about 100 μm thick were manufactured by extrusion-blowing. For improving the bubble stability, the films were actually coextruded with a 10 μm thick film of low density polyethylene that was easily peeled off after processing. The two-line coextrusion device was equipped with an annular die of inner diameter = 120 mm and die gap = 1.2 mm. The average temperature of the melt in both single screw extruders was 270 °C, the die being heated at 250 °C. The screw speed of the nylon6 extruder was 70 rpm and the flow rate 1.8 kg/h. The take up and blow up ratios were 20 and 2, respectively. At the exit of the die, the film was cooled down by blowing air at the base of the die. The films were immediately stored in dry place.

The actual MMT content of the NCs was determined by thermogravimetric analysis (TGA) on a Q50 apparatus from TA Instruments. Oxygen was introduced at 90 mL/min in the oven close to the sample of about 15 mg. Nitrogen was flushed at a 10 mL/min rate from the column head. The temperature range 20−900 °C was scanned at a heating rate of 10 °C/min. The MMT weight fraction in the NCs was assessed from the mass of residue at 900 °C.

Transmission electron microscopy (TEM) observations have been carried out on a FEI Tecnai G2-20 apparatus equipped with a LaB6 filament. About 90 nm thin slices have been prepared from the bulk samples using a Leica ultramicrotome at −30 °C. The TEM bright field micrographs were recorded under an acceleration voltage of 200 kV.

Nuclear magnetic resonance (NMR) experiments have been performed on a Bruker Avance 400 MHz spectrometer. Measurements of proton longitudinal relaxation time, T_1^H, were carried out in static mode at the Magic Angle Spinning using the saturation−recovery sequence with direct proton detection. The Bloch decay spectra consisted of 8 accumulated scans with time laps of 10 s between consecutive scans. The magnetization recovery curves were analyzed with biexponential equations giving a fit confidence ≥95%.

Differential scanning calorimetry (DSC) has been performed on a Perkin-Elmer DIAMOND apparatus. The temperature and heat flow scales were calibrated using high purity tin and indium. The sample weight was in the range 5−10 mg. The data of crystallinity index, X_c, and crystallization temperature, T_c, were average values computed from 3−5 experiments.

Wide-angle X-ray scattering (WAXS) experiments were performed using a INEL 2000 generator equipped with a copper target 2kW X-ray tube. WAXS intensity profiles from isotropic samples were recorded via a curved position-sensitive counter from INEL, using a graphite-monochromated α-radiation. 2D-WAXS patterns were also recorded on a CCD camera from Photonic Science Ltd. In this instance, radial WAXS intensity profiles were obtained by azimuthal integration using the FIT2D software.

Dynamic mechanical analyses (DMA) have been carried out in tensile mode on a RSA equipment from TA Instrument at a frequency of 1 Hz, using a static strain of 1% and a dynamic strain of 0.5%. The strip samples cut out from blown films were 22 and 4 mm in gauge length and width. The temperature range −100/+150 °C was scanned at a heating rate of 1 °C/min.

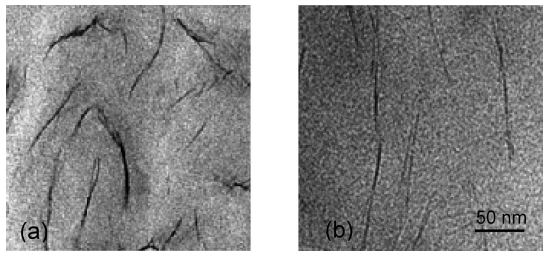

Figure 1. TEM micrographs of PA6-2: (a) as-received pellets; (b) after microextrusion.

Table 2. Relaxation Times, T_1^H, for the PA6-0 and PA6-2 Samples Before and After Microextrusion (∗ Holds for As-Received)

material	T_1^H(s)
PA6-0∗ as-received pellets	2.17
PA6-0 microextruded	2.06
PA6-2∗ as-received pellets	1.4
PA6-2 microextruded	1.08

Results and Discussion

Preliminary Characterization. Considering the dramatic incidence of thermomechanical treatments on the crystallization behavior of NCs, all the materials were submitted to the same processing conditions via microextrusion, including the neat PA6 and the UBE-supplied NCs. Pellets of the as-received materials were also studied for the sake of comparison. Table 1 reports the materials list together with the expected MMT contents and the actual ones as determined from TGA,

The TEM micrographs of Figure 1 show that the MMT particles in the PA6-2 sample are quite well dispersed in the PA6 matrix in the form of thin tactoids, for both the as-received pellets and after microextrusion. WAXS experiments displayed not any signs of the characteristic signature from intercalated MMT particles (see the Blown Films subsection). In the case of the microextruded pellets, the slightly lower thickness of the MMT tactoids suggests that microextrusion improved the MMT dispersion, somewhat.

The MMT dispersion has also been qualitatively studied via solid state NMR spectroscopy following Van der Hart and collaborators' method[45] that benefits from the paramagnetic property of the Fe^{3+} ions of the MMT platelets which speeds up the longitudinal relaxation of the matrix protons close to the platelet surface. The better the clay dispersion, the shorter the average distance between neighbor platelets, and the higher is the paramagnetic contribution to the proton relaxation. The relaxation time, T_1^H, is computed from the final region of the magnetization recovery curves for which a steady-state polarization gradient is assumed for the various proton spins.[74] The data for the PA6-0 and PA6-2 materials are reported in Table 2.

Microextrusion has no significant effect on the T_1^H of PA6-0 within the experimental accuracy. The significant drop of T_1^H for the as-received PA6-2∗ in comparison with the as-received PA6-0∗ is yet relevant to the paramagnetic effect of the Fe^{3+} ions of highly dispersed MMT platelets. Regarding the microextruded PA6-2 sample, the additional T_1^H drop with regard to the as-received counterpart may be ascribed to a better MMT platelet dispersion owing to the additional shearing treatment in the microextruder. This finding supports the previous TEM observations.

The WAXS patterns from the microextruded PA6-0 and PA6-2 are shown in Figure 2. In spite of the rather fast cooling in air of the samples at the exit of the die, PA6-0 is thoroughly crystallized in the α-form, as revealed by the two scattering peaks at $2\theta \approx 20°$ and $2\theta \approx 24°$ associated with the α(200) and α(002/202) planes.[75] This crystal form is the one generated

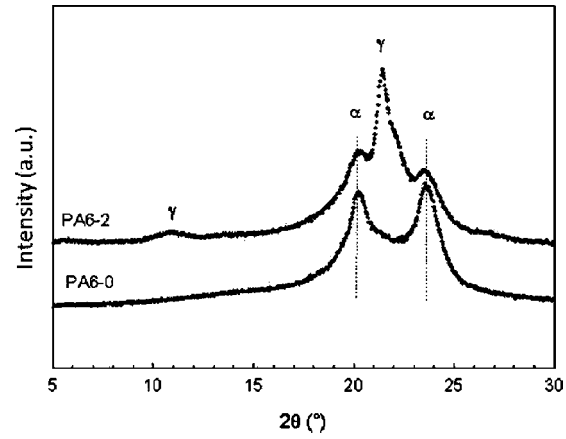

Figure 2. WAXS profiles of the PA6-0 and PA6-2 samples after microextrusion.

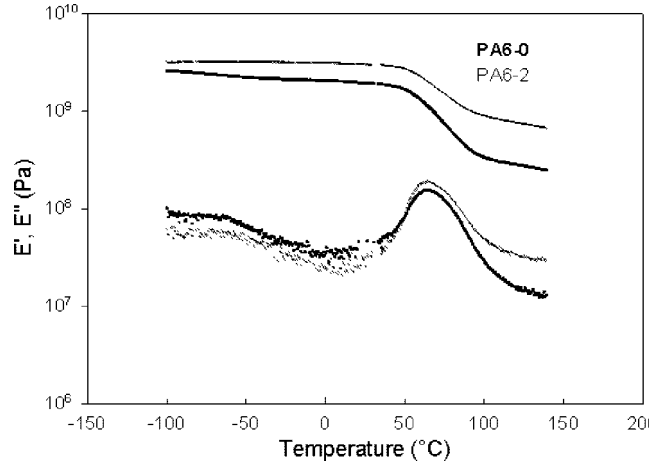

Figure 3. Storage and loss moduli versus temperature for PA6-0 and PA6-2 blown films.

at either high crystallization temperature or slow cooling rates.[76] In contrast, PA6-2 displays mixed α- and γ-crystals and equivalent cooling rate after microextrusion, the scattering peak at $2\theta \approx 21.5°$ being characteristic of the γ(001/200) planes, according to Arimoto's unit cell.[77] This latter finding is consistent with the generally reported γ-nucleating effect of MMT.

Figure 3 shows the variation with temperature of the storage and loss moduli of PA6-0 and PA6-2. The main mechanical relaxation associated with the glass transition of the PA6 matrix in PA6-2 is quite similar to that of neat PA6-0, in agreement with several reports regarding nylon6-clay NCs.[12,18,62] This means that the overall chain mobility is not much sensitive to the presence of MMT platelets in spite of the high dispersion level. If specific interactions have actually been shown to set up between PA6 chains and MMT platelets,[44,46,78] these interactions should necessarily vanish within very short distance away from the platelet surface.

Influence of Microextrusion on Crystallization Kinetics and Crystalline Forms. It is well-known that the melt temperature of nylons has a strong incidence on their crystallization kinetics. It is mandatory to keep the molten material at temperature far beyond the thermodynamic melting point to erase all memory effects due to thermomechanical treatments [see ref 79 and the refs cited therein]. The literature data regarding the crystallization kinetics of nylon6-MMT NCs have been obtained under different conditions that unfortunately do not enable relevant comparison between the various sources.

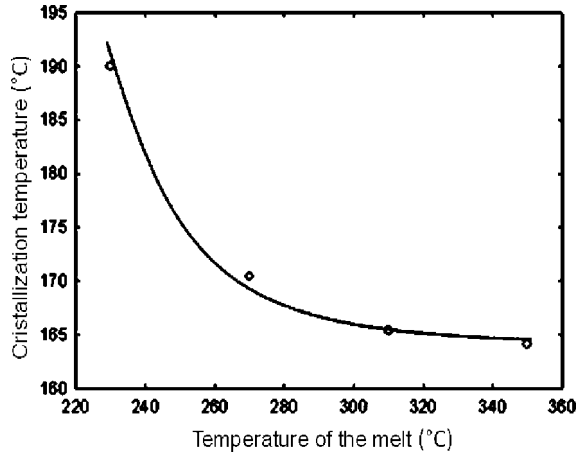

Figure 4. Peak crystallization temperature of as-received PA6-0 versus temperature of the melt (cooling rate, 10 °C/min; holding time prior to cooling, 5 min).

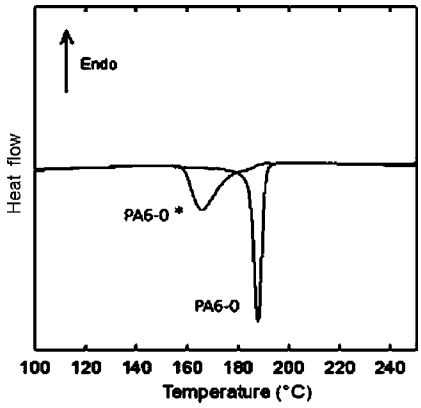

Figure 5. DSC cooling traces of the as-received PA6-0∗ and the microextruded PA6-0 (melt maintained 5 min at 310 °C prior to cooling at 10 °C/min).

Figure 4 shows the peak crystallization temperature, T_c, of as-received PA6-0∗ recorded during cooling from the melt at a cooling rate of 10 °C/min, after holding the melt for 5 min at various temperatures. The Tc values drastically drop with increasing melt temperature before to level off around 165 °C. This means that early crystallization can occur at a rather high temperature if the melt is heated at 230 °C, that is, just above its melting point, owing to some *surviving* ordered regions that promote nucleation, otherwise self-nucleation. In contrast, if the melt temperature is increased beyond 310 °C, the low and nearly constant T_c data suggest that crystallization takes places from homogeneous nucleation, irrespective of the temperature of the melt prior to the cooling step. This limiting temperature will be used as a reference temperature in the aim of erasing the thermomechanical history of the PA6 and NCs samples prior to the crystallization investigations.

The incidence of microextrusion on crystallization kinetics is first checked in Figure 5 for PA6-0. In addition to the much lower crystallization temperature of PA6-0∗ ($T_c \approx 165$ °C) as compared with PA6-0 ($T_c \approx 187$ °C), the crystallization exotherm is much broader. Both findings suggest generation of microextrusion-induced nuclei that speed up the overall crystallization process. Moreover, these finding give clear evidence that if maintaining the melt at 310 °C for 5 min enables erasing the self-seeding nuclei of the as-received PA6-0∗ sample, microextrusion generates organized regions that partly survive this heat treatment.

Considering the rather large Tc gap of the PA6-0∗ and PA6-0 samples, one may wonder about their respective crystalline

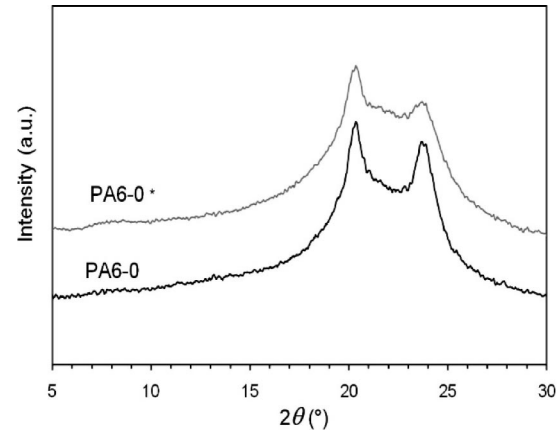

Figure 6. WAXS patterns of the as-received PA6-0∗ and the microextruded PA6-0 directly picked up from the DSC pans after the crystallization experiments of Figure 5.

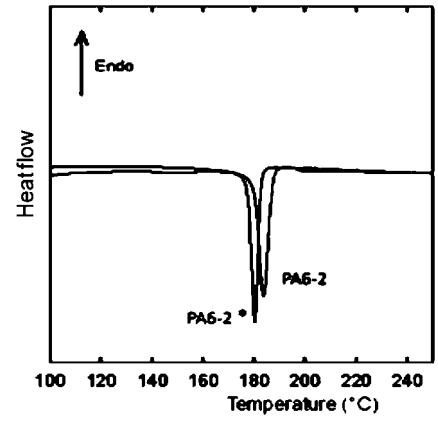

Figure 7. DSC cooling traces of the as-received PA6-2∗ and the microextruded PA6-2 (melt maintained 5 min at 310 °C prior to cooling at 10 °C/min).

structure. Figure 6 shows the WAXS patterns of the PA6-0∗ and PA6-0 directly collected from the DSC experiments of Figure 5. Both samples display the typical scattering rings of the α-crystal form. This is due to the fact that the T_c values of the two materials (Figure 5) fall in the characteristic crystallization range of the α-form under slow cooling conditions from quiescent melt.[76]

The incidence of microextrusion on the NCs crystallization kinetics is further checked in Figure 7 regarding PA6-2∗ and PA6-2. The crystallization temperature of PA6-2 is only increased by +5 °C with respect to PA6-2∗, the peak shape being almost the same. Microextrusion has much less impact on NCs crystallization in comparison with neat PA6.

In Figure 8 are reported the WAXS patterns of the PA6-2∗ and PA6-2 samples collected from the DSC experiments of Figure 7. The as-received PA6-2∗ predominantly crystallizes in the γ-form, which is consistent with both $T_c \approx 180$ °C and the previously mentioned γ-nucleating effect of the MMT platelets. In contrast, PA6-2 exclusively crystallizes into the α-form, in spite of not too much different crystallization parameters. It is yet worth noticing that if the T_c value of PA6-2∗ is much higher than that of PA6-0∗, giving evidence of the γ-nucleating effect of the MMT platelets, the T_c value of PA6-2 is much similar to that of PA6-0, suggesting that the MMT platelets have little if any nucleating effect after microextrusion. In the NCs, the shear-induced nuclei from microextrusion are likely to promote the α-form crystallization as in the case of PA6-0, at $T_c \approx 185$ °C. Considering the rather small T_c gap between the PA6-2∗ ($T_c \approx 180$ °C) and PA6-2 ($T_c \approx 184$ °C),

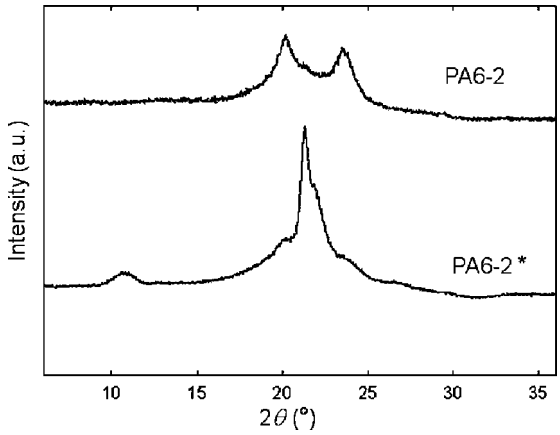

Figure 8. WAXS patterns of the as-received PA6-2∗ and the microextruded PA6-2 directly picked up from the DSC pans after the crystallization experiments of Figure 7.

Table 3. Crystallization Temperature, T_c, for the Various Microextruded Samples[a]

T_c (°C)	PA6-0	PA6-2	PA6-4.5
as-received (∗)	165.0	180.2	179.6
5 rpm	185.2	181.0	182.4
50 rpm	186.8	184.2	182.6

[a] Melt maintained 5 min at 310 °C; cooling rate 10 °C/min; T_c standard deviation is 0.3°C.

one could notwithstanding expect some γ-nucleating effect from the MMT surface in the meantime α-crystallization proceeds. The reason for the missing of γ-crystals in PA6-2 may be the shear amplification effect of the MMT platelets reported by Cakmak and collaborators[40,41] that is likely to enhance the promotion of α-form nuclei. The shear amplification effect should be particularly efficient close to the MMT platelet surface, so that any chance of γ-nucleation and growth from the MMT platelets should be obliterated at 180 °C.

To get better insight into the shear-induced nucleating effect, two levels of microextrusion at 5 and 50 rpm have been checked on PA6-0, PA6-2, and PA6-4.5. The T_c data for the various samples are reported in Table 3. In the case of PA6-0, a 5 rpm screw speed involves a significant T_c increase with regard to PA6-0∗ that suggests the generation of organized region having high nucleating potential. It reveals that the phenomenon already discussed above for the screw speed 50 rpm may occur at rather low shear rates. A similar observation can be made regarding the PA6-4.5 sample, although the T_c increase of the two microextruded samples with respect to the as-received one is not so high. In contrast, microextrusion of PA6-2 at 5 rpm brings about a less stronger T_c increase than at 50 rpm.

The T_c departure of the various samples may be connected with their crystal structure habits in relation to experimental conditions. PA6-0 always crystallizes in the α-form, irrespective of thermomechanical treatment tested in the present study (Figure 6). PA6-2 displays the two crystal forms in various amounts depending on processing as shown in Figure 9. When microextruded at 5 rpm, PA6-2 crystallizes in mixed α- and γ-forms. This situation is intermediate between PA6-2∗ and PA6-2 microextruded at 50 rpm which crystallize in predominant γ- and α-forms, respectively. This comparison allows concluding that 5 rpm generates much less self-seeding nuclei than the 50 rpm screw speed and that these nuclei are not numerous enough to make the α-crystallization invade the entire PA6 matrix during the cooling step. Some opportunities are afforded to γ-form nucleation and growth from the MMT platelets leading to mixed α- and γ-crystals in the final solid material.

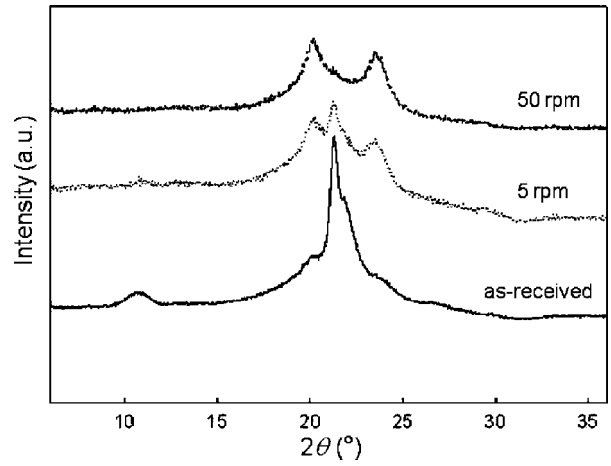

Figure 9. WAXS profiles of PA6-2 samples having various thermomechanical history (melt maintained 5 min at 310 °C prior to cooling at 10 °C/min).

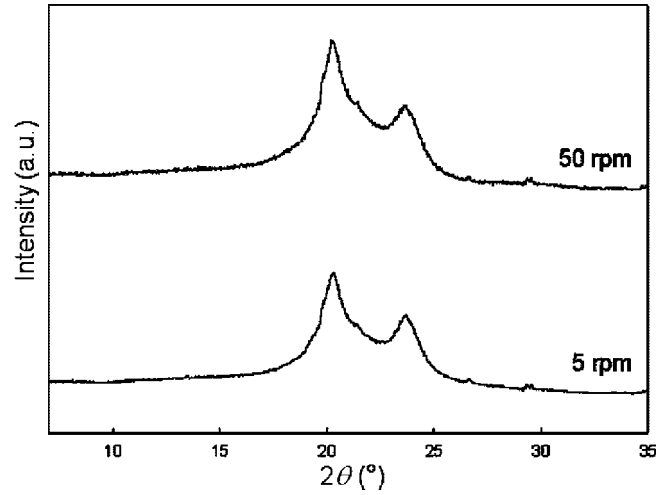

Figure 10. WAXS profiles of PA6-4.5 samples having various thermomechanical history (melt maintained 5 min at 310 °C prior to cooling at 10 °C/min).

Regarding PA6-4.5, only α-crystals are observed after microextrusion at either 5 or 50 rpm, as shown in Figure 10. This means that the 5 rpm screw speed already generates a great number of self-seeding nuclei in PA6-4.5 that prohibit γ-nucleation from the MMT platelets. The reason for this may be again the shear amplification effect of the MMT platelets that is obviously stronger in PA6-4.5 than in PA6-2 due to the higher MMT content: the higher the shear amplification, the higher the capabilities for self-seeding nucleation at the same screw speed.

Influence of MMT on Nonisothermal Crystallization. Considering the above conclusion that thermomechanical history cannot be thoroughly erased after holding the melt at 310 °C for 5 min, all materials have been microextruded prior to any investigation, using the same processing parameters. Figure 11 shows the crystallization temperature of neat PA6 and NCs under slow cooling from the melt versus MMT content. The monotonic T_c drop suggests a MMT-induced hindrance to crystal growth. It is to be noticed that, as a result of the slow cooling crystallization, all the materials display the α-crystal form, as can be observed on the WAXS profiles of Figure 12. This latter finding is not only consistent with the T_c values that stand in the temperature range favorable to α-crystal growth[76] but also stresses the dominant role of the self-nucleation over the MMT-

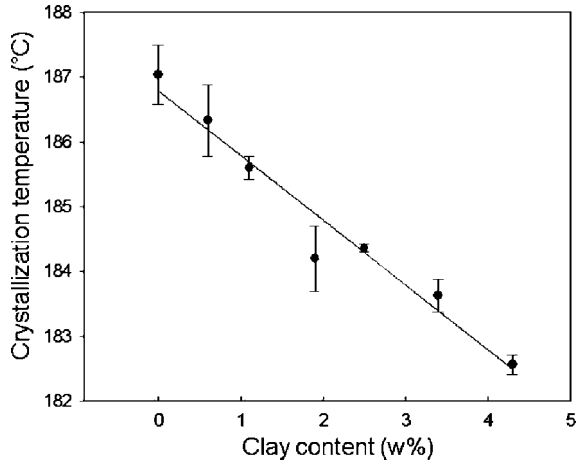

Figure 11. Crystallization temperature of the NCs as a function a MMT content at constant cooling rate after microextrusion (crystallization parameters: heating rate 10 °C/min from RT up to 310 °C; melt held 5 min at 310 °C; cooling rate 10 °C/min).

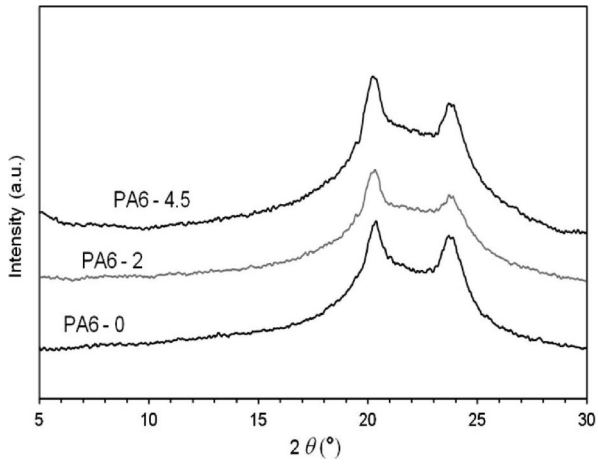

Figure 12. WAXS profiles of the microextruded PA6-0, PA6-2 and PA6-4.5 directly picked up from the DSC pans after the crystallization experiments of Figure 11.

induced heterogeneous nucleation in the case of slow cooling. Both T_c data and WAXS observations are contradictory to some previous studies which report a steady increase of the peak crystallization temperature of PA6-clay NCs in parallel with the so-called γ-nucleating effect.[44,46] Our findings seem better consistent with Fornes and Paul[37] and Homminga et al. as well.[59] Fornes and Paul's reported that extruded NCs disclosed a striking acceleration of isothermal crystallization kinetics at low clay contents, then a slowing down of crystal growth at clay contents beyond 1% by weight. However, in contrast to the present data, most of the NCs crystallization rates reported by the latter authors remained greater than that of the corresponding pure matrix: this is evidence that introducing MMT platelets improves nucleation with respect to neat nylon6 but increasing the MMT content restricts crystal growth.[27,59] This is corroborated by small-angle X-ray scattering data from Lincoln et al.[80] showing a gradual loss the regular lamellar stacking with increasing MMT content. Unfortunately, neither the crystal form of the extruded pellets nor that of the DSC crystallized samples was reported in Fornes and Homminga studies so that the crystallization mechanism cannot be discussed further. The structural analysis was only performed on injection-molded samples[37] that displayed largely predominant γ-crystals in the skin region and mixed α- and γ-crystals in the core region. The cooling rate in the sample skin was obviously higher than in the present study, resulting in γ-crystal growth. To sum up, the

Table 4. Crystallinity of the Microextruded Samples Crystallized from the Melt at a Cooling Rate of 10 °C/Min[a]

materials	PA6-0	PA6-0.5	PA6-1	PA6-2	PA6-2.5	PA6-3.5	PA6-4.5
crystallinity (w%)	33.1	31.7	31.3	31.4	33.5	33.4	32.4

[a] Data computed from the crystallization exotherm of the DSC cooling scans.

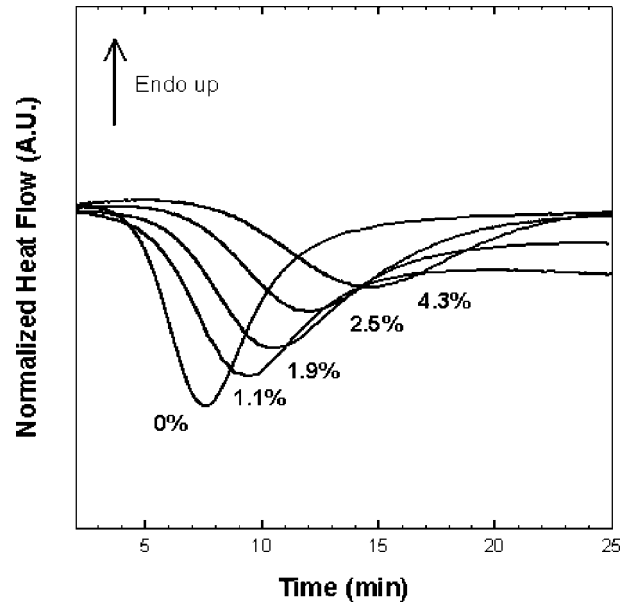

Figure 13. Isothermal crystallization of microextruded PA6 and NCs at 203 °C (melt held 5 min at 310 °C; cooling at 135 °C/min down to 203° prior to isothermal crystallization).

data from the various independent studies give evidence that the natural crystallization habits of PA6 in relation to the crystallization conditions may turn predominant over the induced effects of filler and thermomechanical history. The roughly invariant crystallinity of the samples, as can be seen in Table 4, is quite consistent with this statement. However, one may conclude from the present data that, besides the competition between self- and induced nucleation effects, a strong hindrance to crystal growth due to the MMT platelets is responsible for the reduced crystallization rate of the NCs.

Isothermal crystallization experiments have been carried out at 203 °C to get complete transformation within reasonable time. The DSC heat flow versus time curves for the various NCs are reported in Figure 13, and the crystallization half-time data versus MMT content are plotted in Figure 14. Isothermal crystallization of the PA6 matrix is obviously slowing down ith increasing MMT content in the NCs (Figure 13). The crystallization half-time of PA6-4.5 is roughly twice that of neat PA6 (Figure 14). This corroborates the previous conclusion from nonisothermal crystallization that the MMT platelets hinder the crystal growth in the PA6 matrix, yet without reducing the final crystallinity.

The WAXS profiles of three of the isothermally crystallized samples are reported in Figure 15. All three samples exhibit the α-crystal form typical of nylon6 crystallization at high temperature,[76] and nylon6 NCs as well.[81] In spite of the rather long time afforded to the crystallization (Figure 13), the γ-nucleation potential of the MMT platelets was thoroughly inhibited as in the previous case of slow cooling. This finding cannot be taken as an evidence that shear-induced nucleation predominates over MMT-induced nucleation, however, it seriously contradicts Medellin-Rodriguez et al.'s claim that "shear does not affect the induction of the γ-form attributed to the presence of exfoliated clay".[25]

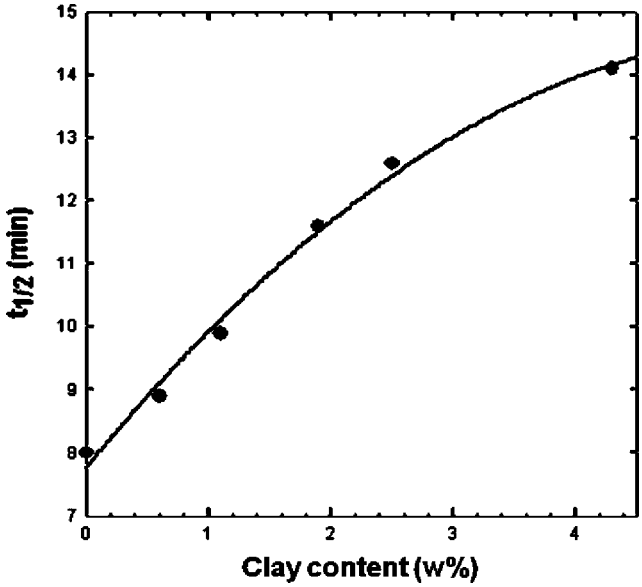

Figure 14. Transformation half-time as a function of MMT content for isothermal crystallization of the NCs at 203 °C.

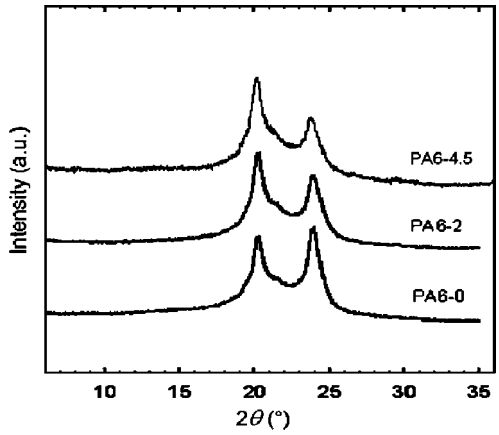

Figure 15. WAXS profiles of the isothermally crystallized samples directly picked up from the DSC pans after the experiments of Figure 13.

Incidence of MMT on Fast Cooling Crystallization. The generation of shear-induced nuclei during microextrusion was shown to promote α-crystallization for PA6-0 and NCs under both isothermal and nonisothermal crystallization, when the latter is carried out at 10 °C/min (see Figures 6, 8, and 15). Figure 16 shows the WAXS profiles of PA6-0 and PA6-2 following fast cooling at 135 °C/min, which are much similar to the ones recorded directly from the extruded samples cooled in air (Figure 2). PA6-0 surprisingly displays the predominance of α-form crystals characteristic of slow cooling crystallization. The reason may be again the shear-induced self-nucleation that is likely to promote crystallization of PA6−0 at higher temperature than without shear, during monotonic cooling.

In contrast, the clear-cut γ-scattering that is observed in the case of PA6-2 is indicative of a strong modification of the crystallization mechanism for this material when the cooling is changed from slow to fast. Considering the previous findings regarding PA6-0 at the cooling rate = 135 °C/min (Figure 16) and PA6-2 at 10 °C/min (Figure 8) that both displayed α-crystals, one may suspect that the driving force for the γ-crystallization of PA6-2 at 135 °C/min is a synergism between the T_c drop due to fast cooling and the γ-nucleating potential of the MMT platelets that inhibits the activity of the shear-induced α-nuclei.

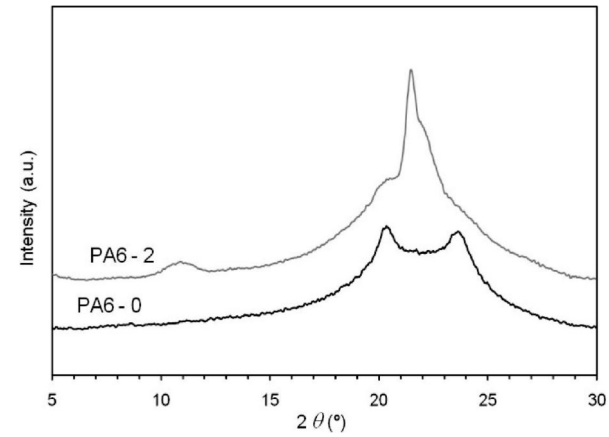

Figure 16. WAXS profiles of the PA6-0 and PA6-2 microextruded samples after crystallization by cooling at 135 °C/min (samples directly picked up from the DSC pans; melt held 5 min at 310 °C prior to the cooling).

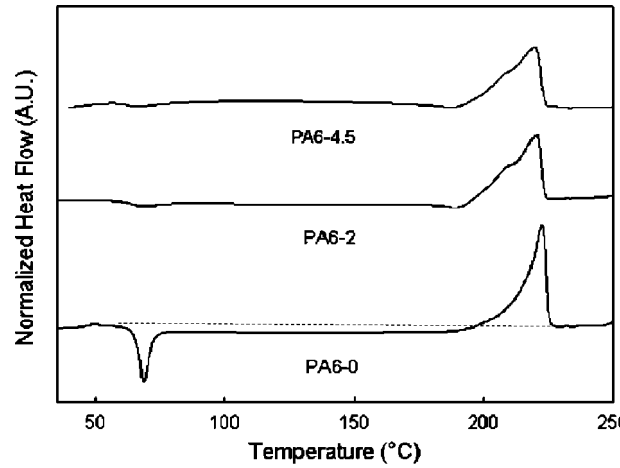

Figure 17. DSC heating scans of the quenched samples at a heating rate of 10 °C/min.

For further exploration of this hypothesis, neat PA6-0 and NCs have been quenched from the melt at 310 °C into isopropanol at 5 °C, that is, below the glass transition temperature of the PA6 matrix, $T_g \approx 55$ °C. The DSC heating scans of the quenched samples are shown in Figure 17. The cold crystallization peak at bout 70 °C for PA6-0 reveals that the cooling rate of the quenching was so high that it largely prevented crystallization. The broad exotherm in the range 80−200 °C can be ascribed to the presence of the mesomorphic β-form that is well-known to transform into α-crystal during the DSC scan.[82,84] In contrast, both PA6-2 and PA6-4.5 only display a very faint cold crystallization peak indicating that crystallization did occur during the quenching, before the sample temperature reached T_g. However, an additional faint exotherm appears about 190 °C for PA6-2 and PA6-4.5, prior to the melting endotherm. According to previous studies,[82,83] this exotherm may be ascribed to the early melting of unstable defective γ-crystals that immediately recrystallize into more stable α-crystals. The hump on the melting peak of the two NCs approximately located at 210 °C is relevant to the presence of stable γ-crystals that melt before the stable α-crystals. To sum up, both the absence of cold crystallization and the presence of the high temperature $\gamma-\alpha$ transition in the DSC heating curves of the NCs give evidence that the MMT platelets have a strong activation effect on the NCs crystallization.

The WAXS spectra of Figure 18 provide more information on the actual structure of the samples after quenching and on

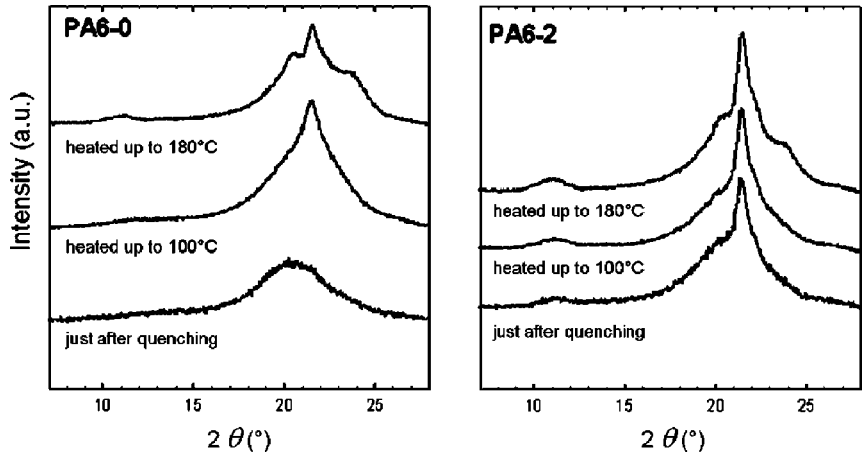

Figure 18. WAXS spectra of PA6-0 and PA6-2 after quenching and subsequently heated up to 100 and 180 °C (heating in the DSC was carried out at 10 °C/ min before cooling at the same rate for correlation with the DSC experiments of Figure 17; the WAXS spectra were recorded at room temperature).

the structural changes that occur during the heating scan. Regarding the PA6-0 sample, a broad scattering halo characteristic of the amorphous state is observed just after quenching. The presence of the mesomorphic β-form unfortunately cannot be confirmed due to overlapping with the amorphous scattering.[84] The heating up to 100 °C generates a sharp scattering peak at $2\theta \approx 21.5°$ that is relevant to the growth of γ-crystals during the cold-crystallization process.[85] Heating up to 180 °C involves the appearance of two additional peaks characteristic of the α-crystal form at $2\theta \approx 20°$ and $2\theta \approx 24°$. Because the γ-scattering is barely affected upon heating from 100 to 180 °C (Figure 18), the growth of α-crystals is much likely the result of the β-α transformation in this temperature range.[82] Finally, considering that no distinct hump characteristic of the γ-crystal melting can be seen on the typical α-melting endotherm of Figure 17, one may suspect that the unstable γ-crystals underwent a $\gamma-\alpha$ transition in the range 180−220 °C. In strong contrast with PA6-0, the quenched PA6-2 sample exhibits the characteristic γ-scattering at $2\theta \approx 21.5°$ (Figure 18) that corroborates the occurrence of crystallization during the quenching, before chain immobilization below T_g. The additional presence of the γ-reflection at $2\theta \approx 11°$, unresolved for PA6-0 after the cold crystallization, gives indication that this crystalline form has better perfection in quenched PA6-2 than in cold-crystallized PA6-0. No α-crystals can be seen in quenched PA6-2. Heating up to 100 °C does not change the WAXS profile, in agreement with the DSC scan of Figure 17, which indicates very minor cold-crystallization. However, the heating of PA6-2 up to 180 °C results in two humps on both sides of the main γ-scattering that are relevant to the growth of a few α-crystals. Considering that 180 °C is just before the occurrence of the premelting exotherm, it is much likely that these α-crystals again arose from a $\beta-\alpha$ transition rather than from a $\gamma-\alpha$ transition. The quite sharper and more intense γ-scattering of PA6-2 as compared with PA6-0 after the heating up to 180 °C points out the greater perfection of this crystalline species in the former material, in agreement with the observation of γ-crystal true melting on the DSC trace at about 210 °C (Figure 17). It is worth noticing that the unreported WAXS data regarding PA6-4.5 revealed very similar behavior as PA6-2. It can be thus concluded that the MMT particles have a strong acceleration effect on the NCs crystallization during quenching. The previous evidence that the overall growth rate can be strongly reduced in case of slow cooling or isothermal crystallization emphasize the prime role of the nucleation step in quenched crystallization. Besides, the γ-nucleating effect of MMT already pointed out in the case of fast cooling at 135 °C/min is thoroughly corroborated.

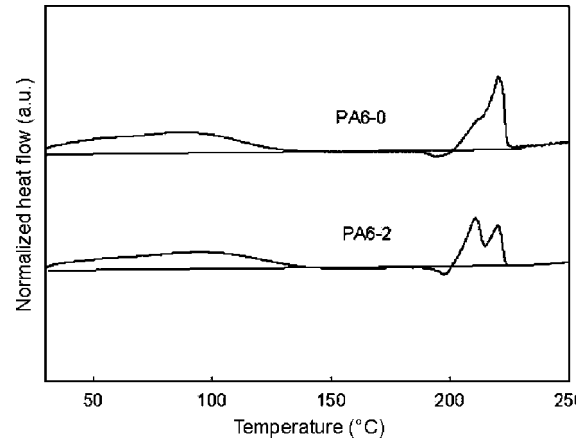

Figure 19. DSC heating curves of the PA6-0 and PA6-2 blown films.

It is worth noticing that Liu et al.[29] reported absolutely similar results regarding the effect of quenching at various cooling rates on the crystalline form of neat PA6 and NCs of various MMT contents: NCs systematically displayed γ-crystallization whereas neat PA6 turned out to be amorphous. These authors argued that the specific interactions between the MMT platelets and the PA6 chains are likely to the promote the chain-twisted conformation characteristic of the γ-crystal.

Blown Films. PA6-0 and PA6-2 films manufactured by extrusion-blowing offer an opportunity to investigate additional combination of processing parameters.

The DSC heating curve of the PA6-0 film reported in Figure 19 displays three major features: a prominent α-crystal melting peak at 220 °C, an exotherm about 190 °C assigned to the $\gamma-\alpha$ transformation of defective γ-crystals, and a hump at about 210 °C on the main melting peak that is relevant to the true melting of well-ordered γ-crystals. The DSC heating curve of the PA6-2 blown film is strongly distinguished from that of the PA6-0 film in the melting temperature range that exhibits an intense true γ-crystal melting peak at 210 °C and a reduced α-crystal melting peak at 220 °C. Considering that a part of the latter α-crystals results from the $\gamma-\alpha$ transition evidenced through the 190 °C exotherm, it is quite clear that γ-crystals are largely predominant in the PA6-2 film.

The 2D-WAXS patterns of Figure 20 reveal a perfect isotropy for the crystalline structure of the MMT-free PA6-0 film. This structural feature is relevant to (1) a strong capability of the

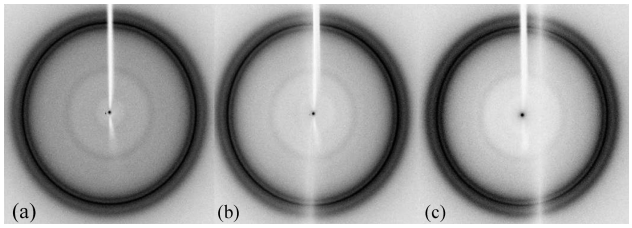

Figure 20. 2D-WAXS patterns of the PA6-0 blown film: (a) through-view; (b) edge-view; (c) end-view (sample vertical for the b and c patterns).

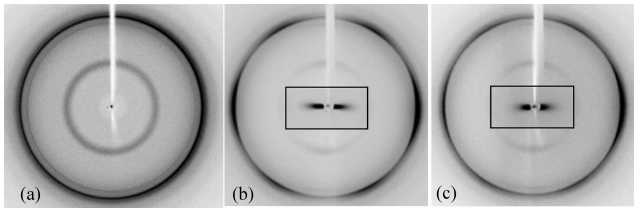

Figure 21. 2D-WAXS and SAXS patterns (enlarged central window) of the PA6-2 blown film: (a) through-view; (b) edge-view; (c) end-view (sample vertical for the b and c patterns).

PA6 chains to relax completely during the blow-stretching step of the process, prior to solidification and (2) no preferred crystal growth direction due to thermal gradient or film surface effects. Although the actual cooling rate of the film could not be determined, it obviously should be rather fast. Indeed, the concomitant growth of α- and γ-crystals in the PA6-0 blown film is indicative of a situation intermediate between the quenching and the fast cooling at 135 °C/min of the microextruded sample reported in the previous subsection. The very strong γ-reflection between the two α-reflections of moderate intensity corroborates the DSC analysis that γ-crystals are predominant.

Regarding the PA6-2 blown film, the through-view of the 2D-WAXS patterns reported in Figure 21 reveals very faint α-reflections on both sides of the very strong γ-reflection, in perfect agreement with the DSC observations of largely predominant γ-crystals. These γ-crystals seem isotropically distributed in the PA6 matrix. However, the edge- and end-view WAXS patterns of Figure 21 disclose a very strong orthotropic texturing of γ-crystals. In addition, the central windows of the edge- and end-view patterns exhibit an intense equatorial small-angle X-ray scattering (SAXS) that is relevant to MMT platelets highly oriented parallel to the film surface.

Both the WAXS from the PA6 matrix and the SAXS from the MMT platelets are quite similar to Kojima et al.'s observations regarding an extruded cast film of nylon6-MMT hybrid containing 0.74% vol. of MMT.[21] The monotonic decrease of the equatorial SAXS intensity with increasing scattering angle, without evidence of a correlation maximum arising from intercalated tactoids[86] in the range of scattering vector 0.5 $nm^{-1} < q < 5\ nm^{-1}$ (in Figure 21b), is a strong hint in support of the high degree of MMT dispersion.

The γ-crystal texturing of the PA6-2 blown film is analyzed in more details in Figure 22 that reports the "equatorial" and the "30°-azimuth" profiles from the edge-view pattern of Figure 21b. The major γ-peak of both profiles occurs at $2\theta \approx 21°$, that is, the typical angular position of the γ(001) reflection, with a marked asymmetry assigned to the γ(200) reflection on the high-angle side of the peak. In contrast to Kojima et al.'s findings, the present 2D patterns are clearly relevant to a double texturing of the PA6 matrix with crystals matching the MMT platelet surface on either the γ(001) or the γ(200) plane, the chain axis lying flat on the platelets in both cases.

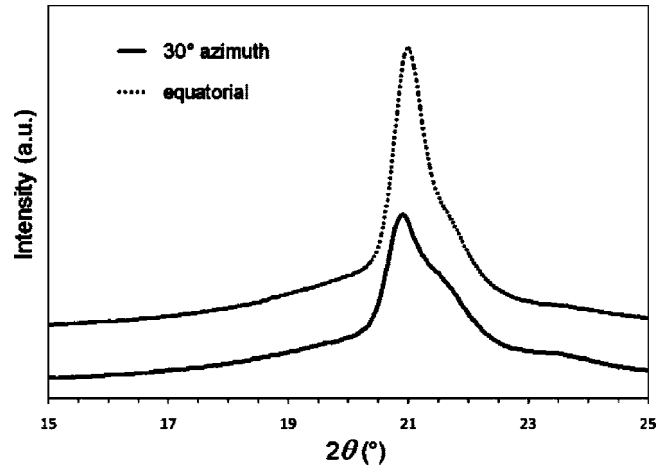

Figure 22. "Equatorial" and "30°-azimuth" radial profiles from the edge-view WAXS pattern of Figure 21b (azimuthal integration over ± 10° for both radial profiles).

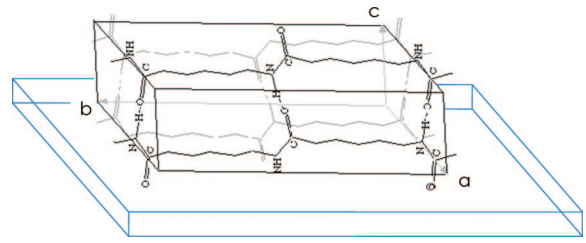

Figure 23. Sketch of the γ(001) texturing parallel to the MMT platelet surface in the NCs blown films.

The first situation is sketched in Figure 23, with chains anchored to the platelets via their amide groups, and the H-bonded sheets of the γ-unit cell standing up onto the MMT platelets. This is precisely the kind of epitaxial arrangement suggested by Maiti and Okamoto[28] without experimental evidence. These authors argued that the rather good matching of the crystallographic *b*-parameter along the chain axis of the nylon6 γ-form and the average distance between OH groups on the MMT platelet surface may be the driving force of the epitaxial growth. The corresponding contributions of this crystallographic arrangement to the WAXS pattern of Figure 21b are the equatorial (001) and the quadrant (200) reflections. The complementary contributions to the Figure 21b pattern, that is, the quadrant (001) and the equatorial (200) reflections, are relevant to γ-crystals with their (200) planes stacked parallel to the MMT surface. This is not really consistent with an epitaxial growth since true epitaxy should have resulted in a single crystallographic stacking. Therefore, if the preferred γ(001) texturing parallel to the MMT platelet surface (Figure 23) can reasonably be ascribed to the MMT epitaxial nucleation, the γ(200) texturing should be assigned another origin, namely the shear-amplified chain orientation in the PA6-2 blown film with regard to the neat PA6 film. Experimental evidence have been provided by Medellin-Rodriguez et al.[25] that, after applying a shear deformation to the melt, the relaxation of oriented chains in NCs is much longer than in neat nylon6. In the present circumstances, the eventual activation of shear-induced α-nuclei was strongly inhibited by the fast cooling which promotes γ-crystallization, as in the case of the neat PA6 film (Figure 20). The reason why shear-induced molecular orientation should favor the γ(200) plane alignment parallel to the MMT surface away from the MMT platelet surface is that, under shear deformation, crystalline polymers undergo planar texturing of the crystallographic plane having the lower critical shear stress.[87] The H-bonded sheets having weak van der Waals interactions

between the planes are precisely such low critical shear stress planes in the γ-crystal unit cell of PA6. Considering that most of the H-bonds exist in dynamic equilibrium in molten polyamides,[88] the combination of melt shear and slow chain relaxation in NCs[25] is likely to promote orientation of both chains and H-bonds in the shear plane, making thus a template for the incipient crystallization of the oriented H-bonded sheets. Afterward, crystallization kinetics determines which crystalline form will grow in the pretextured material, namely the γ-form in the case of fast cooling. This is typically the case of both nylon6 and nylon6/MMT fibers spun at not too high take up speed,[89,90] the NCs spun fibers being more chain-oriented than the neat PA6 fibers at equivalent spinning conditions.[90] Therefore, the double texturing of the PA6−2 blown film should be the result of two competing processes: 1) the epitaxial growth of the MMT-nucleated γ-crystals on the oriented MMT platelet, i.e. the γ-(001) texturing, and 2) the development of shear-induced γ-crystals in the PA6 matrix between the exfoliated MMT platelets, i.e. the γ-(200) texturing.

Concluding Remarks

The main issues of the study are the following: (1) The MMT platelets have an actual γ-nucleating effect on the PA6 matrix. The local chain organization on the MMT platelets is likely to govern the γ-nucleation capabilities involving chain-twisted conformations, as already suggested by Maiti and Okamoto.[28] This MMT-induced property is enhanced upon fast cooling due to the natural propensity of PA6 for γ-crystallization below 100 °C. This situation is particularly encountered in the case of quenching. (2) The γ-nucleating potentiality of MMT may be yet thoroughly or partly inhibited by the shear-induced self-nucleation that promotes α-crystallization. In microextruded samples, shear-induced self-nuclei with preferred chain-extended conformations promote an early α-form crystallization beyond 180 °C in the case of slow cooling. The growth of α-crystals is expected to proceed away from the potentially γ-nucleating MMT platelets, in agreement with Vanderhart et al.'s findings from NMR.[45] Besides, α-crystallization always predominates at high T_c, irrespective of MMT content and shear effect. (3) The reduction of the global crystallization kinetics in the case of slow cooling or isothermal crystallization is relevant to the hindrance of the MMT platelets to the growth of α-form lamellae. These α-crystals have yet enough time to grow before the occurrence of γ-crystals owing to the very low crystallization kinetics of the latter ones at high T_c. (4) Increasing the concentration of the potentially γ-nucleating MMT involves an increase of the shear-amplification phenomenon that is likely to promote the α-form self-nucleation in parallel. This is an additional factor of competition between the two crystal species.

To sum up, the growth of α- and γ-form crystals having more or less connections with the MMT platelets in the polymer matrix of PA6-MMT NCs is a competing process ruled out by a combination of the following factors: the MMT content, the shear intensity of the molten material during processing, the melt temperature prior to solidification, and the cooling rate.

The apparent contradiction between the MMT-induced reduction of the overall growth rate in the case of slow cooling or isothermal crystallization and the acceleration of the process in the case of fast cooling emphasizes the competition between nucleation and growth, given that γ-crystals grow much faster than α-crystals below about 100 °C.[76] In other words, fast cooling stimulates the γ-nucleating character of the MMT platelets so that the overall PA6 crystallization rate in the NCs is higher than without MMT. In contrast, slow cooling promotes the activation of the shear-induced α-nuclei accompanied with a reduction of the NCs crystallization rate due to the MMT hindrance to crystal growth. This analysis is consistent with several studies[24,37,40] that reported predominant γ-crystals in the skin region of injection-molded NCs and predominant α-crystals in the core region. It also applies to the crystallization behavior of MMT-PA6 fibers that exhibit γ-crystal structure after melt-spinning and α-crystal structure when spun NCs fibers are slow cooled from the unconstrained melt.[47]

Based on a few WAXS experiments regarding the crystallization of nylon6-MMT NCs under either shear or quiescent conditions, Medellin-Rodriguez et al.[25] concluded that shear does not affect the induction of the γ-crystallization which is mainly attributed to the presence of exfoliated clay. The authors' explanation was that shear promotes the chain-extended conformation that is ascribed to the γ-form, whereas the α-form is associated with chain-folded crystals. This assumption is based on the fact that the γ-form is commonly observed in spun fibers whereas the α-form is predominant for quiescent crystallization. There are three major points that contradict this statement. First, though nylon6 fiber spinning usually results in predominant γ-form,[89−93] very high spinning rates do promote the α-form.[89,93] Second, nylon6 drawn fibers always exhibit predominant α-crystals[90−92] whereas γ-crystals can be grown from quiescent melt provided that crystallization is carried out below 100 °C or upon fast cooling.[76] Third, the α-form has a planar zigzag chain conformation, that is, chain-extended,[74] whereas the γ-form has chain-twisted conformation, that is, not chain-extended.[77] If Medellin-Rodriguez et al.'s experiments cannot be disputed, the interpretation of the data regarding the shear effect is erroneous and the present work shows that, due to its effect on local chain organization and owing to the dynamic H-bonding of the chains in the melt, shear may actually inhibit the γ-crystal growth from the MMT platelets depending of the shear intensity and the subsequent crystallization conditions.

Acknowledgment. The Centre National de la Recherche Scientifique and the Région Nord/Pas-de-Calais are deeply acknowledged for the grant of a doctoral fellowship to F.P. The authors are also indebted to the Région Nord/Pas-de-Calais and the European FEDER Program (ARCir Contract N°04/060/031) and the University of Lille for funding to the X-ray CCD camera equipment. Deep thanks are addressed to Prof. S. Bourbigot for help in the NMR analysis and to Dr. A. Addad for the TEM experiments.

References and Notes

(1) Giannelis, E. P. *Adv. Mater.* **1996**, *8*, 29–35.
(2) Lefebvre, J.-M. In *Encyclopedia of Polymer Science and Technology*, 3rd edition; Kroschwitz, J. I., Mark, H. F., Eds.; John Wiley & Sons: New York, 2003; Vol. *3*, pp 336−352.
(3) Usuki, A.; Hasegawa, N.; Kato, M. *Adv. Polym. Sci.* **2005**, *179*, 135–195.
(4) Chazeau, L.; Gauthier, C.; Vigier, G.; Cavaille, J. Y. In *Handbook of Organic-Inorganic Hybrid Materials and Nanocomposites*; Nalwa, H. S., Ed.; American Sciences Publishers; Stevenson Ranch, CA, 2003; Vol. *2*.
(5) Sengupta, R.; Chakraborty, S.; Bandyopadhyay, S.; Dasgupta, S.; Mukhopadhyay, R.; Auddy, K.; Deuri, A. *Polym. Eng. Sci.* **2007**, *47*, 1956–74.
(6) Stretz, H. A.; Paul, D. R. *Polymer* **2006**, *47*, 8123–8136.
(7) Sepehr, M.; Utracki, L. A.; Zheng, X.; Wilkie, C. A. *Polymer* **2005**, *46*, 11569–11581.
(8) Wang, D.; Zhu, J.; Yao, Q.; Wilkie, C. A. *Chem. Mater.* **2002**, *14*, 3837–3843.
(9) Le Pluart, L.; Duchet, J.; Sautereau, H. *Polymer* **2005**, *46*, 12267–12278.
(10) Ganguli, S.; Dean, D.; Jordan, K.; Price, G.; Vaia, R. *Polymer* **2003**, *44*, 1315–1319.
(11) Nam, P. H.; Maiti, P.; Okamoto, M.; Kotaka, T.; Hasegawa, N.; Usili, A. *Polymer* **2001**, *42*, 9633–9640.
(12) Masenelli-Varlot, K.; Vigier, G.; Vermogen, A.; Gauthier, C.; Cavaille, J.-Y. *J. Polym. Sci., Part B: Polym. Phys.* **2007**, *45*, 1243–1251.
(13) Sun, T.; Garces, J. M. *Adv. Mater.* **2002**, *14*, 128–130.
(14) Tsai, T.-Y.; Li, C.-H.; Chang, C.-H.; Cheng, W.-H.; Hwang, C.-L.; Wu, R.-J. *Adv. Mater.* **2005**, *17*, 1769–1773.

(15) Pegoretti, A.; Kolarik, J.; Peroni, C.; Migliaresi, C. *Polymer* **2004**, *45*, 2751–2759.
(16) Ray, S. S.; Maiti, P.; Okamoto, M.; Kazunobu, T.; Yamada, K.; Ueda, K. *Macromolecules* **2002**, *35*, 3104–10.
(17) Kojima, Y.; Usuki, A.; Kawasumi, M.; Okada, A.; Fukushima, Y.; Kurauchi, T.; Kamigaito, O. *J. Mater. Res.* **1993**, *8*, 1185–1189.
(18) Xie, S.; Zhang, S.; Wang, F.; Liu, H.; Yang, M. *Polym. Eng. Sci.* **2005**, *45*, 1247–1253.
(19) Liu, X.; Wu, Q. *Macromol. Mater. Eng.* **2002**, *287*, 180–186.
(20) Fornes, T. D.; Paul, D. R. *Macromolecules* **2004**, *37*, 7698–7709.
(21) Kojima, Y.; Usuki, A.; Kawasumi, M.; Okada, A.; Kuraichi, T.; Kamigaito, O.; Kaji, K. *J. Polym. Sci., Part B: Polym. Phys.* **1994**, *32*, 625–630.
(22) Liu, L.; Qi, Z.; Zhu, X. *J. Appl. Polym. Sci.* **1999**, *71*, 1133–1138.
(23) Lincoln, D. M.; Vaia, R. A.; Wang, Z.-G.; Hsiao, B. S.; Krishnamoorti, R. *Polymer* **2001**, *42*, 9975–9985.
(24) Varlot, K.; Reynaud, E.; Kloppfer, M.-H.; Vigier, G.; Varlet, J. *J. Polym. Sci., Part B: Polym. Phys.* **2001**, *39*, 1360–1370.
(25) Medellin-Rodriguez, F. J.; Burger, C.; Hsiao, B. S.; Chu, B.; Vaia, R.; Philips, S. *Polymer* **2001**, *42*, 9015–9023.
(26) Wang, S.; Hu, Y.; Li, Z.; Wang, Z.; Zhuang, Y.; Chen, Z.; Fan, W. *Colloid Polym. Sci.* **2003**, *281*, 951–956.
(27) Lincoln, D. M.; Vaia, R. A.; Krishnamoorti, R. *Macromolecules* **2004**, *37*, 4554–4561.
(28) Maiti, P.; Okamoto, M. *Macromol. Mater. Eng.* **2003**, *288*, 440–445.
(29) Liu, X.; Wu, Q.; Berglund, L. A.; Qi, Z. *Macromol. Mater. Eng.* **2002**, *287*, 515–522.
(30) Nair, S. S.; Ramesh, C. *Macromolecules* **2005**, *38*, 454–462.
(31) Bertmer, M.; Wang, M.; Kruger, M.; Blumich, B.; Litvinov, V. M.; van Es, M. *Chem. Mater.* **2007**, *19*, 1089–1097.
(32) Murase, S.; Inoue, A.; Miyashita, Y.; Kimura, N.; Nishio, Y. *J. Polym. Sci., Part B: Polym. Phys.* **2002**, *40*, 479–487.
(33) Xie, S.; Zhang, S.; Wang, F.; Yang, M.; Seguela, R.; Lefebvre, J.-M. *Compos. Sci. Technol.* **2007**, *67*, 2334–41.
(34) Zheng, J.; Siegel, R. W.; Toney, C. G. *J. Polym. Sci., Part B: Polym. Phys.* **2003**, *41*, 1033–1050.
(35) Rawal, A.; Fang, X.-W.; Urman, K.; Iverson, D.; Otaigbe, J. U.; Schmidt-Rohr, K. *J. Polym. Sci., Part B: Polym. Phys.* **2008**, *46*, 857–860.
(36) Chae, D. W.; Oh, S. G.; Kim, B. C. *J. Polym. Sci., Part B: Polym. Phys.* **2004**, *42*, 790–799.
(37) Fornes, T. D.; Paul, D. R. *Polymer* **2003**, *44*, 3945–396.
(38) Zapata-Espinosa, A.; Medellin-Rodriguez, F. J.; Stribeck, N.; Almendarez-Camarillo, A.; Vega-Diaz, S.; Hsiao, B. S.; Chu, B. *Macromolecules* **2005**, *38*, 4246–4253.
(39) Wu, T.-M.; Chen, E. C.; Liao, C. S. *Polym. Eng. Sci.* **2002**, *42*, 1141–1150.
(40) Yalcin, B.; Valladares, D.; Cakmak, M. *Polymer* **2003**, *44*, 6913–6925.
(41) Yalcin, B.; Cakmak, M. *Polymer* **2004**, *45*, 2691–2710.
(42) Wu, T.-M.; Liao, C. S. *Macromol. Chem. Phys.* **2000**, *201*, 2820–2825.
(43) Xie, S.; Zhang, S.; Liu, H.; Chen, G.; Feng, M.; Qin, H.; Wang, F.; Yang, M. *Polymer* **2005**, *46*, 5417–5427.
(44) MacDonald, I.; Ginic-Markovic, M.; Clarke, S.; Matisons, J.; Wu Dong, Y. *ACS Symposium Series 978*; American Chemical Society: Washington, DC, 2008; pp 261276.
(45) VanderHart, D. L.; Asano, A.; Gilman, J. W. *Chem. Mater.* **2001**, *13*, 3796–3809.
(46) Wu, Q.; Liu, X.; Berglund, L. A. *Polymer* **2002**, *43*, 2445–2449.
(47) Ibanes, C.; de Boissieu, M.; David, L.; Seguela, R. *Polymer* **2006**, *47*, 5071–5079.
(48) Reynaud, E.; Jouen, T.; Gauthier, C.; Vigier, G.; Varlet, J. *Polymer* **2001**, *42*, 8759–68.
(49) Zhao, C.; Zhang, P.; Lu, S.; He, J.; Wang, X. *J. Mater. Sci.* **2007**, *42*, 9083–9091.
(50) Ramasundaram, S. P.; Kim, K. J. *Macromol. Symp.* **2007**, *249−250*, 295–302.
(51) Murthy, N. S.; Kotliar, A. M.; Sibilia, J. P.; Sacks, W. *J. Appl. Polym. Sci.* **1986**, *31*, 2569–82.
(52) Sano, M.; Sasaki, D. Y.; Kunitake, T. *Science* **1992**, *258*, 441–3.
(53) Saeed, K.; Park, S.-Y. *J. Appl. Polym. Sci.* **2007**, *106*, 3729–35.
(54) Li, J.; Fang, Z.; Tong, L.; Gu, A.; Liu, F. *J. Polym. Sci., Part B: Polym. Phys.* **2006**, *44*, 1499–1512.
(55) Zeng, H.; Gao, C.; Wang, Y.; Watts, P. C.; Kong, H.; Cui, X.; Yan, D. *Polymer* **2006***47*, 113–122.
(56) Liu, T.; Phang, I. Y.; Shen, L.; Chow, S. Y.; Zhang, W.-D. *Macromolecules* **2004**, *37*, 7214–22.
(57) Avella, M.; Errico, M. E.; Gentile, G. *Macromol. Symp.* **2006**, *234*, 170–175.
(58) Liu, X.; Wu, Q. *Eur. Polym. J.* **2002**, *38*, 1383–1389.
(59) Homminga, D. S.; Goderis, B.; Mathot, V. B. F.; Groeninckx, G. *Polymer* **2006**, *47*, 1630–1639.
(60) Miltner, H. E.; Van Assche, G.; Pozsgay, A.; Pukanszky, B.; Van Mele, B. *Polymer* **2006**, *47*, 826–835.
(61) Ray, S. S.; Okamoto, M. *Prog. Polym. Sci.* **2003**, *28*, 1539–1641.
(62) Vlasveld, D. P. N.; Groenewold, J.; Bersee, H. E. N.; Picken, S. J. *Polymer* **2005**, *46*, 12567–12576.
(63) VanderHart, D. L.; Asano, A.; Gilman, J. W. *Chem. Mater.* **2001**, *13*, 3781–3795.
(64) Lee, Y.-H.; Bur, A. J.; Roth, S. C.; Start, P. R. *Macromolecules* **2005**, *38*, 3828–3837.
(65) Vaia, R. A.; Giannelis, E. P. *MRS Bull.* **2001**, *26*, 394–401.
(66) Winberg, P.; Eldrup, M. M.; Pedersen, N. J.; van Es, M. A.; Maurer, F. H. J. *Polymer* **2005**, *46*, 8239–8249.
(67) Fornes, T. D.; Paul, D. R. *Polymer* **2003**, *44*, 4993–5013.
(68) Chavarria, F.; Paul, D. R. *Polymer* **2004**, *45*, 8501–15.
(69) Sheng, N.; Boyce, M. C.; Parks, D. M.; Rutledge, G. C.; Abes, J. I.; Cohen, R. E. *Polymer* **2004**, *45*, 487–506.
(70) Weon, J.-I.; Sue, H.-J. *Polymer* **2005**, *46*, 6325–34.
(71) Varlot, K.; Raynaud, E.; Vigier, G.; Varlet, J. *J. Polym. Sci., Part B: Polym. Phys.* **2002**, *40*, 272–283.
(72) Kim, G. M.; Lee, D. H.; Hollmann, B.; Kressler, J.; Stoppelmann, G. *Polymer* **2001**, *42*, 1095–1100.
(73) Usuki, A.; Kojima, Y.; Kawasumi, M.; Okada, A.; Fukushima, Y.; Kurauchi, T.; Kamigaito, O. *J. Mater. Res.* **1993**, *8*, 1179–84.
(74) Bourbigot, S.; VanderHart, D. L.; Gilman, J. W.; Awad, W. H.; Davis, R. D.; Morgan, A. B.; Wilkie, C. A. *J. Polym. Sci., Part B: Polym. Phys.* **2003**, *41*, 3188–3213.
(75) Holmes, D. R.; Bunn, C. W.; Smith, D. J. *J. Polym. Sci.* **1955**, *17*, 159–177.
(76) Kyotani, M.; Mitsuhashi, S. *J. Polym. Sci., Part B: Polym. Phys.* **1972**, *10*, 1497–1508.
(77) Arimoto, H.; Ishibashi, M.; Hirai, M.; Chatani, Y. *J. Polym. Sci., Gen. Pap.* **1965**, *3*, 317–326.
(78) Usuki, A.; Koiwai, A.; Kojima, Y.; Kawasumi, M.; Okada, A. *J. Appl. Polym. Sci.* **1995**, *55*, 119–123.
(79) Xenopoulos, A.; Clark, E. S. In *Nylon Plastics Handbook*; Kohan, M. I., Ed.; Hanser Publishers; Munich, 1995; Chapter *5*.
(80) Lincoln, D. M.; Vaia, R. A.; Wang, Z. G.; Hsiao, B. S. *Polymer* **2001**, *42*, 1621–1631.
(81) Wu, T. M.; Lien, Y. H.; Hsu, S. F. *J. Appl. Polym. Sci.* **2004**, *94*, 2196–2204.
(82) Penel-Pierron, L.; Debecker, C.; Seguela, R.; Lefebvre, J. M. *J. Polym. Sci., Part B: Polym. Phys.* **2001**, *39*, 484–495.
(83) Medellin-Rodriguez, F. J.; Larios-Lopez, L.; Zapata-Espinoza, A.; Davalos-Montoya, O.; Phillips, P. J.; Lin, J. S. *Macromolecules* **2004**, *37*, 1799–1809.
(84) Persyn, O.; Miri, V.; Lefebvre, J. M.; Ferreiro, V.; Brink, T.; Stroeks, A. *J. Polym. Sci., Part B: Polym. Phys.* **2006**, *44*, 1690–1701.
(85) Khanna, Y. P.; Kuhn, W. P. *J. Polym. Sci., Part B: Polym. Phys.* **1997**, *35*, 2219–31.
(86) Vaia, R. A. In *Polymer-Clay Nanocomposites*; Pinnavaia, T. J., Beall, G. W., Eds; John Wiley & Sons: New York, 2000; Chapter 12.
(87) Seguela, R. *J. Macromol. Sci., Polym. Rev.* **2005**, *45*, 263–287.
(88) Skrovanek, D. J.; Painter, P. C.; Coleman, M. M. *Macromolecules* **1986**, *19*, 699–705.
(89) Ergungor, Z.; Cakmak, M.; Batur, C. *Macromol. Symp.* **2002**, *185*, 259–276.
(90) Ibanes, C.; David, L.; de Boissieu, M.; Seguela, R.; Epicier, T.; Robert, G. *J. Polym. Sci., Part B: Polym. Phys.* **2004**, *42*, 3876–3892.
(91) Stepaniak, R. F.; Garton, A.; Carlsson, D. J.; Wiles, D. M. *J. Polym. Sci., Part B: Polym. Phys.* **1979**, *17*, 987–99.
(92) Gianchandani, J.; Spruiell, J. E.; Clark, E. S. *J. Appl. Polym. Sci.* **1982**, *27*, 3527–51.
(93) Murase, S.; Kashima, M.; Kudo, K.; Hirami, M. *Macromol. Chem. Phys.* **1997**, *198*, 561–572.

MA801804Y